11-1-2017

Influence of the megathrust earthquake cycle on upper-plate deformation in the Cascadia forearc of Washington State, USA

Jaime E. Delano
Western Washington University

Colin B. Amos
Western Washington University

John P. Loveless
Smith College, jloveles@smith.edu

Tammy M. Rittenour
Utah State University

Brian L. Sherrod
University of Washington

See next page for additional authors

Authors
Jaime E. Delano, Colin B. Amos, John P. Loveless, Tammy M. Rittenour, Brian L. Sherrod, and Emerson M. Lynch

Influence of the megathrust earthquake cycle on upper plate deformation in the Cascadia forearc of Washington State

Jaime E. Delano[1], Colin B. Amos[1], John P. Loveless[2], Tammy M. Rittenour[3], Brian L. Sherrod[4], and Emerson M. Lynch[2]

[1]Department of Geology, Western Washington University, 516 High Street, Bellingham, Washington 98225, USA

[2]Department of Geosciences, Smith College, 44 College Lane, Northampton, Massachusetts 01063, USA

[3]Department of Geology, Utah State University, 4505 Old Main Hill, Logan, Utah 84322, USA

[4]U.S. Geological Survey, Department of Earth and Space Sciences, University of Washington, Box 351310, Seattle, Washington 98195, USA

ABSTRACT

The influence of subduction zone earthquake cycle processes on permanent forearc deformation is poorly understood. In the Cascadia subduction zone forearc of Washington State, deformed and incised fluvial terraces serve as archives of longer-term (10^3-10^4 yr) strain manifest as both fluvial incision and slip on upper-plate faults. We focus on comparing these geomorphic records in the Wynoochee River valley in the southern Olympic Mountains with short-term (10^1 yr) deformation driven by interseismic subduction zone coupling. We use optically stimulated luminescence dating and high-resolution elevation data to characterize strath terrace incision and differential uplift across the Canyon River fault, which cuts Wynoochee River terraces. This analysis demonstrates reverse slip rates of ~0.1–0.3 mm/yr over the past ~12–37 ky, which agree with rates predicted by a GPS-constrained boundary element model of interseismic stress from Cascadia subduction zone coupling. Similarly, model-predicted patterns of interseismic uplift mimic the overall pattern of incision in the lower Wynoochee River valley, as revealed by strath elevations dated at 14.1 ± 1.2 ka. Agreement between modeled short-term and observed long-term records of forearc strain suggests that interseismic stress drives slip on upper-plate faults and fluvial incision in Cascadia. Consistency over multiple time scales may indicate relative stability in spatial patterns of subduction zone coupling over at least ~10^4 yr intervals.

INTRODUCTION

A comprehensive picture of deformation, topographic development, and seismic hazard in subduction zone forearcs requires understanding strain over multiple time intervals. Although interseismic deformation above a subduction zone is considered to be largely elastic (e.g., Mazzotti et al., 2002; Mitchell et al., 1994), some fraction may be retained as permanent strain over multiple earthquake cycles (e.g., Kelsey et al., 1994; Melnick et al., 2009). Records of incremental deformation preserved in Quaternary forearc landforms may encode information about the relative stability of shorter-term (10^1-10^3 yr) processes such as interseismic strain, segmentation of megathrust ruptures, and upper-plate faulting (Personius, 1995).

The relationship between deformation from the megathrust earthquake cycle and Holocene-active forearc faults and folds is poorly quantified. Forearc structures may accommodate margin-normal and/or parallel slip related to the orientation of plate convergence (e.g., McCaffrey, 1993) and may be sensitive to stress induced by great subduction earthquakes (Aron et al., 2013; Loveless and Pritchard, 2008). Accordingly, megathrust earthquakes may trigger slip on forearc faults (Sherrod and Gomberg, 2014), or conversely, ruptures on upper-plate structures may initiate subduction earthquakes by decoupling the megathrust (González et al., 2015). Forearc structures may also serve as boundaries that control the length and location of subduction zone ruptures over multiple earthquake cycles (Melnick et al., 2009).

In this study, we quantify deformation in the Wynoochee River valley in the southern Olympic Mountains of Washington State (Fig. 1) using lidar data, optically stimulated luminescence (OSL) dating, and cm-scale terrace-strath surveys. We calculate longer-term ($\geq 10^3$ yr) slip on the upper-plate Canyon River fault (CRF) and fluvial downcutting for comparison with decadal-scale, modeled interseismic deformation from the Cascadia subduction zone (CSZ). We utilize a boundary element method (Crouch and Starfield, 1983; Thomas, 1993) model to infer upper-plate fault slip needed to relieve stress from subduction zone coupling estimated from GPS observations, as well as regional interseismic uplift. Together, these results provide an explicit examination of links between CSZ-related deformation, forearc fault slip, and fluvial incision.

BACKGROUND

Geodetic measurements show that the CSZ accommodates NE-SW oblique convergence between the Juan de Fuca and N. American plates (Fig. 1 inset). Geodetic-geomorphic comparisons in Oregon imply that small amounts of interseismic strain persist over multiple earthquake cycles, rather than being entirely elastic (Kelsey et al., 1994). Permanent deformation in the CSZ forearc reflects some combination of slip on upper-plate faults (e.g., Wells et al., 1998), wedge accretion manifest as underplating or aseismic folding (Hyndman and Wang, 1993; Pazzaglia and Brandon, 2001), and poorly understood contributions from the megathrust earthquake cycle.

Records of uplift in the Olympic Mountains, the topographic high of the CSZ forearc, include both thermochronologic measurements at ~10^6 yr time scales (Brandon et al., 1998) and river incision records at ~10^3-10^5 yr scales (Pazzaglia and Brandon, 2001). These studies demonstrate that incision rates broadly agree with longer term exhumation rates, implying steady-state erosion over millennial and perhaps longer time scales.

Within the Olympic Peninsula are east and NE-striking reverse, strike-slip, and oblique-slip faults that together accommodate trench-parallel shortening implied by obliquity in plate convergence (Fig. 1) (e.g., Barnett et al., 2015; Blakely et al., 2009; Witter et al., 2008). Previous studies in Cascadia proposed that upper-plate fault slip arises from the deficit between plate convergence and trench-normal megathrust earthquake rebound (e.g., Mazzotti et al., 2002; Wang et al., 1995). Alternatively, curvature in the subducting slab (Bevis et al., 2001) and associated oroclinal bending could focus interseismic trench-parallel shortening on upper-plate structures (Allmendinger et al., 2005).

The NE-striking CRF represents one such fault in the southern Olympic Mountains (Fig. 1), accommodating south-side-up reverse or oblique motion (Walsh and Logan, 2007), similar to faults in Puget Lowlands (Fig. 1). Airborne lidar (Quinault River Basin, 2012; Southwest Washington, 2009) reveals a previously unmapped strand of the CRF that cuts terraces along the Wynoochee River, a prominent N-S drainage with headwaters in the southern Olympic Mountains (Figs. 1 and 2). The Wynoochee River basin contains several generations of alpine glacial moraines, aggradational fills and glaciolacustrine deposits, and degradational strath terraces (Carson, 1970). To explore potential links between the geomorphology of this area and the CSZ earthquake cycle, we compare the record of faulting and incision to deformation from interseismic subduction zone coupling.

DECADAL AND MILLENNIAL SLIP ON THE CANYON RIVER FAULT

Our mapping of the CRF reveals a segmented, steeply south-dipping fault with south-side-up reverse displacement indicated by offset terraces. The emergence of a narrow canyon and associated knickpoint downstream of the fault (Figs. 2 and 3b) is also consistent with south-side-up displacement as the stream must narrow, steepen, and incise to compensate for relatively faster uplift (e.g., Amos and Burbank, 2007). We mapped eight generations of terraces (Qt1 to Qt8), some containing minor subset cut-in-fill terraces denoted by 'b' and 'c.' We calculate dip-slip rate on the CRF using topographic profiles extracted from the lidar, OSL ages (Table 1) derived from standard sampling and lab procedure (Figs. DR1-DR8; Appendix DR1), and fault dip estimated from trenching (Walsh and Logan, 2007). Though Walsh and Logan (2007) observed oblique, sinistral-reverse slickenlines on the CRF ~10 km to the east, no laterally offset features are observed in the Wynoochee valley.

Topographic profiles along terrace surfaces cut by the CRF (Fig. 2, profiles A-P) yield vertical separations of ~0.9–6.1 m (Fig. 2a; Table DR3, Appendix DR1). In combination with OSL ages from the Qt8, Qt7, and Qt4 terraces (Table 1), these measurements suggest vertical separation rates of ~0.1–0.4 ± 0.1 mm/yr (Fig. 2a, Table DR3). Uncertainty in matching the Qt5 terrace across the CRF yields vertical separations of 4.3 ± 1.6–7.7 ± 3.5 m, depending on the continuity of the northern terrace tread with

Qt5 and Qt5b south of the fault (Fig. 2c). These profiles give vertical separation rates of 0.3 + 0.2/-0.1 and 0.5 + 0.3/-0.2 mm/yr, respectively, using the offset Qt5 deposit age of 14.8 ± 2.0 ka (WYN-06). Based on a range of fault dips from 55 to 85ºS, encompassing the observed 70°S dip from Walsh and Logan (2007), the median reverse slip rate for all profiles is 0.2 mm/yr (Table DR3). Since OSL sample burial predates modern tread formation, OSL-derived separation rates are regarded as minima (Appendix DR1).

To test the relationship between slip on the CRF and the underlying CSZ, we use a boundary element method model (e.g., Crouch and Starfield, 1983) to calculate stress imposed on the CRF by interseismic coupling on the CSZ (Fig. DR9) estimated using a geodetically constrained block model (Meade and Loveless, 2009). We then estimate slip rates on the CRF required to relieve the imposed stress, assuming that the CRF is a shear traction-free surface (details in Appendix DR1), similar to studies of the San Andreas fault system (e.g., Cooke and Dair, 2011). The resulting slip rate distribution represents that of CRF earthquake(s) normalized by recurrence interval, assuming slip completely relieves accumulated shear stress imposed by CSZ coupling. Using a nominal 70ºS fault dip and 10 km fault depth, the model predicts south-side-up motion, with estimated reverse slip rates of 0.1–0.5 mm/yr (Fig. DR10). At the Wynoochee River, estimated reverse slip is ~0.1–0.2 mm/yr. The lateral component of estimated slip ranges up to 0.7 mm/yr of dextral motion (Fig. DR10). We tested alternative fault depths and connectivity to consider uncertainty in fault geometry (Appendix DR1). These variations yield the same slip sense (reverse-dextral) and slip rates of similar magnitude and within the geomorphic uncertainty.

INCISION AND UPLIFT OF THE WYNOOCHEE RIVER VALLEY

We use terrace strath incision along the Wynoochee River to estimate long-term (10^3-10^4 yr) vertical uplift and compare to modeled interseismic uplift (Fig. 3). This analysis uses the elevation of the Qt5 strath, the most continuous and best-exposed terrace in the Wynoochee valley. Strath heights come from high-resolution differential GPS field surveys and well log data (Table DR4) (Washington State Dept. of Ecology, 2015). In the upper reaches of the Wynoochee River (<20 km), the Qt5 terrace deposit contains a thick aggradational fill (~5–20 m) deposited on fine-grained glaciolacustrine deposits and basalt (Fig. 3b). Incised glacial deposits beneath Qt5 fill suggest alternating periods of vertical incision, aggradation, and valley re-excavation, resulting in artificially high incision rates. We therefore focus on the overall rate and pattern of incision in the lower reaches of the river (>20 km), where relatively thin fluvial deposits overlie straths incised into sedimentary bedrock (Fig. 3b). Here, OSL dates provide the minimum strath abandonment age and therefore maximum incision rates (e.g., Litchfield and Berryman, 2006).

Incision of the Qt5 strath, calculated by subtracting the channel elevation from the strath elevation, varies along the length of the Wynoochee River (Fig. 3c). Discrepancy between strath offset and Qt5 terrace tread offset (~4–7 m, Fig. 2c) across the CRF supports our inference of diachronous strath cutting below Qt5 in the glacially influenced, upper reaches of the river (<20 km). Where strath incision is potentially more straightforward to interpret downstream, the Qt5 strath shows broad warping over a half wavelength of ~30 km (Fig. 3c). The range of Qt5 strath heights incised into sedimentary bedrock corresponds to incision rates of 0.4 ± 0.3–1.8 ± 0.3 mm/yr, assuming simultaneous tread abandonment and using an average Qt5 OSL age of 14.1 ± 1.2 ka (Fig. 3c, Appendix DR1).

Modeled uplift rates representing combined effects of CSZ coupling and CRF slip are ~2.1–2.8 mm/yr along the Wynoochee valley (Fig. 3a,c). This total rate reflects interseismic uplift plus an average annual contribution from CRF earthquakes. Interseismic uplift rates generally decrease to the east with increasing distance from strong CSZ coupling (Fig. DR11), but south-side-up motion on the CRF introduces some deviation from this pattern. Notably, the Wynoochee River flows through a local minimum in model-predicted uplift, owing to segmentation of the CRF within the valley (Fig. 3a).

DISCUSSION

Similarities in rates and patterns of Late Pleistocene faulting and incision and the predicted deformation from the model suggest that interseismic subduction zone coupling may drive permanent forearc fault slip and uplift. On the CRF, reverse slip rates inferred from terrace offsets (~0.2 mm/yr; Fig. 2) closely match the model rates (0.1–0.2 mm/yr) (Fig. 3a). These rates are consistent with those of similarly oriented structures in the SE Olympic Mountains, including the Saddle Mountain fault, which displays post-glacial vertical deformation rates of ~0.2 mm/yr (Barnett et al., 2015).

The general match in reverse slip rates across multiple timescales suggests that interseismic stress from the coupled subduction zone may alone cause upper-plate fault slip in the forearc; no additional driving mechanisms, such as CSZ coseismic slip (Figs. DR13–14, Appendix DR1) or crustal block motions, are required to produce the observed reverse slip on the CRF. The predicted component of dextral slip on the CRF from the model, however, does not match observed sinistral-reverse slickenlines (Walsh and Logan, 2007). That said, lateral slip is poorly recorded in Holocene landforms and potentially varies along-strike, between the coseismic and interseismic phase of the megathrust earthquake cycle, and/or over multiple earthquake cycles. As such, we focus here on predicted reverse motion on the CRF driven by subordinate trench-parallel convergence due to subduction zone coupling. Reverse slip on the CRF also compares well with geomorphic evidence of continued, south-side-up reverse motion on the CRF (Fig. 2).

Several factors complicate the degree to which fluvial downcutting recorded by Wynoochee terraces (Fig. 3) reflects tectonic uplift. The presence of aggradational fills and evidence for repeated glaciation, particularly in the upper basin (Carson, 1970), suggest that a component of incision may result from glacial isostatic adjustment from local alpine glaciers and/or the Puget Lobe of the Cordilleran ice sheet (<35 km to the east; Fig. 1) (Thorson, 1989). Additionally, the prevalence of bedrock incision along the entire length of the Wynoochee River (Fig. 3c) reflects climactic factors such as long-term base level lowering from sediment loss at the river mouth (Carson, 1970), or gradient decrease from headwater sediment loss. Incision rates are also calculated over half a glacial cycle, and are thus overestimates. Given these factors, we focus on comparing overall spatial patterns of incision and interseismic uplift rather than the absolute rates.

Neither isostasy nor base level change, however, likely produces the broad, ~15–20 m warping of the Qt5 terrace strath in the lower Wynoochee River (Fig. 3c). Although this feature could reflect motion on a blind fault, we note a correlation between incision and predicted interseismic uplift along the Wynoochee valley (Fig. 3c and inset). Combined with the location of the Wynoochee River at a local minimum in total modeled uplift (Fig. 3a), such spatial coincidence suggests that terrace downcutting mimics short-term strain patterns. This result resembles previous findings based on geomorphic observations in Oregon (Kelsey et al., 1994; Personius, 1995).

Our results imply that long-term (>10^3 yr) forearc deformation, including trench-parallel shortening expressed as reverse faulting, broad scale folding, and uplift of the Olympic Mountains represents a permanent component of interseismic strain. Hence, deformation in the Cascadia forearc could express long-lived, temporally stable patterns of interplate coupling.

ACKNOWLEDGMENTS

We thank Nicola Litchfield, Juliet Crider, Rich Briggs, and anonymous referees for helpful reviews; the Green Diamond Resource Co. for access; the Puget Sound Lidar Consortium for hosting lidar data; and Tabor Reedy, Kaelin Newman, and Scott Bennett for help and discussions in the field. OSL dating was supported by the EarthScope AGeS Program.

REFERENCES CITED

Allmendinger, R.W., González, G., Yu, J., Hoke, G., and Isacks, B., 2005, Trench-parallel shortening in the Northern Chilean Forearc: Tectonic and climatic implications: Geological Society of America Bulletin, v. 117, p. 89–104, doi:10.1130/B25505.1.

Amos, C.B., and Burbank, D.W., 2007, Channel width response to differential uplift: Journal of Geophysical Research, Earth Surface, v. 112, p. F02010, doi:10.1029/2006JF000672.

Aron, F., Allmendinger, R.W., Cembrano, J., González, G., and Yáñez, G., 2013, Permanent fore-arc extension and seismic segmentation: Insights from the 2010 Maule earthquake, Chile: Journal of Geophysical Research, v. 118, p. 724–739, doi:10.1029/2012JB009339.

Barnett, E.A., Sherrod, B.L., Hughes, J.F., Kelsey, H.M., Czajkowski, J.L., Walsh, T.J., Contreras, T.A., Schermer, E.R., and Carson, R.J., 2015, Paleoseismic Evidence for Late Holocene Tectonic Deformation along the Saddle Mountain Fault Zone, Southeastern Olympic Peninsula, Washington: Bulletin of the Seismological Society of America, v. 105, p. 38–71, doi:10.1785/0120140086.

Bevis, M., Kendrick, E., Smalley, R., Brooks, B., Allmendinger, R., and Isacks, B., 2001, On the strength of interplate coupling and the rate of back arc convergence in the central Andes: An analysis of the interseismic velocity field: Geochemistry Geophysics Geosystems, v. 2, p. 1067, doi:10.1029/2001GC000198.

Blakely, R.J., Sherrod, B.L., Hughes, J.F., Anderson, M.L., Wells, R.E., and Weaver, C.S., 2009, Saddle Mountain fault deformation zone, Olympic Peninsula, Washington: Western boundary of the Seattle uplift: Geosphere, v. 5, p. 105–125, doi:10.1130/GES00196.1.

Brandon, M.T., Roden-Tice, M.K., and Garver, J.I., 1998, Late Cenozoic exhumation of the Cascadia accretionary wedge in the Olympic Mountains, northwest Washington

State: Geological Society of America Bulletin, v. 110, p. 985–1009, doi:10.1130/0016-7606(1998)110<0985:LCEOTC>2.3.CO;2.

Carson, R., 1970, Quaternary Geology of the South-Central Olympic Peninsula, Washington [Ph.D. Thesis]: Seattle, Washington, University of Washington, 67 p.

Cooke, M.L., and Dair, L.C., 2011, Simulating the recent evolution of the southern big bend of the San Andreas fault, Southern California: Journal of Geophysical Research, v. 116, p. B04405, doi:10.1029/2010JB007835.

Crouch, S.L., and Starfield, A.M., 1983, Boundary Element Methods in Solid Mechanics: With Applications in Rock Mechanics and Geological Engineering: London, U.K., George Allen & Unwin, 322 p.

González, G., Salazar, P., Loveless, J.P., Allmendinger, R.W., Aron, F., and Shrivastava, M., 2015, Upper plate reverse fault reactivation and the unclamping of the megathrust during the 2014 northern Chile earthquake sequence: Geology, v. 43, p. 671–674, doi:10.1130/G36703.1.

Hyndman, R.D., and Wang, K., 1993, Thermal constraints on the zone of major thrust earthquake failure: The Cascadia Subduction Zone: Journal of Geophysical Research. Solid Earth, v. 98, p. 2039–2060, doi:10.1029/92JB02279.

Kelsey, H.M., Engebretson, D.C., Mitchell, C.E., and Ticknor, R.L., 1994, Topographic form of the Coast Ranges of the Cascadia Margin in relation to coastal uplift rates and plate subduction: Journal of Geophysical Research. Solid Earth, v. 99, p. 12245–12255, doi:10.1029/93JB03236.

Litchfield, N., and Berryman, K., 2006, Relations between postglacial fluvial incision rates and uplift rates in the North Island, New Zealand: Journal of Geophysical Research, Earth Surface, v. 111, p. F02007, doi:10.1029/2005JF000374.

Loveless, J.P., and Pritchard, M.E., 2008, Motion on upper-plate faults during subduction zone earthquakes: Case of the Atacama Fault System, northern Chile: Geochemistry Geophysics Geosystems, v. 9, Q12017, doi:10.1029/2008GC002155.

Mazzotti, S., Dragert, H., Hyndman, R.D., Miller, M.M., and Henton, J.A., 2002, GPS deformation in a region of high crustal seismicity: N. Cascadia forearc: Earth and Planetary Science Letters, v. 198, p. 41–48, doi:10.1016/S0012-821X(02)00520-4.

McCaffrey, R., 1993, On the role of the upper plate in great subduction zone earthquakes: Journal of Geophysical Research. Solid Earth, v. 98, p. 11953–11966, doi:10.1029/93JB00445.

Meade, B.J., and Loveless, J., 2009, Block Modeling with Connected Fault-Network Geometries and a Linear Elastic Coupling Estimator in Spherical Coordinates: Bulletin of the Seismological Society of America, v. 99, p. 3124–3139, doi:10.1785/0120090088.

Melnick, D., Bookhagen, B., Strecker, M.R., and Echtler, H.P., 2009, Segmentation of megathrust rupture zones from fore-arc deformation patterns over hundreds to millions of years, Arauco peninsula, Chile: Journal of Geophysical Research. Solid Earth, v. 114, p. B01407, doi:10.1029/2008JB005788.

Mitchell, C.E., Vincent, P., Weldon, R.J., and Richards, M.A., 1994, Present-day vertical deformation of the Cascadia Margin, Pacific Northwest, United States: Journal of Geophysical Research, v. 99, p. 12257–12277, doi:10.1029/94JB00279.

Pazzaglia, F.J., and Brandon, M.T., 2001, A Fluvial Record of Long-term Steady-state Uplift and Erosion Across the Cascadia Forearc High, Western Washington State: American Journal of Science, v. 301, p. 385–431, doi:10.2475/ajs.301.4-5.385.

Personius, S.F., 1995, Late Quaternary stream incision and uplift in the forearc of the Cascadia subduction zone, western Oregon: Journal of Geophysical Research. Solid Earth, v. 100, p. 20193–20210, doi:10.1029/95JB01684.

Quinault River Basin [lidar file], 2012, Seattle, WA: USGS and Puget Sound Lidar Consortium. Available: Puget Sound Lidar Consortium, Seattle, WA http://pugetsoundlidar.ess.washington.edu/index.htm (accessed September 2014).

Sherrod, B., and Gomberg, J., 2014, Crustal earthquake triggering by pre-historic great earthquakes on subduction zone thrusts: Journal of Geophysical Research. Solid Earth, v. 119, p. 1273–1294, doi:10.1002/2013JB010635.

Southwest Washington [lidar file], 2009, Portland, OR: Oregon Department of Geology and Mineral Industries. Available: Puget Sound Lidar Consortium, Seattle, WA http://pugetsoundlidar.ess.washington.edu/index.htm (accessed September 2014).

Thomas, A., 1993, Poly3D: A three-dimensional, polygonal element, displacement boundary element computer program with applications to fractures, faults, and cavities in the Earth's crust [Ms. Thesis]: Stanford University, 69 p.

Thorson, R.M., 1989, Glacio-isostatic response of the Puget Sound area, Washington: Geological Society of America Bulletin, v. 101, p. 1163, doi:10.1130/0016-7606(1989)101<1163:GIROTP>2.3.CO;2.

Walsh, T.J., and Logan, R.L., 2007, Results of trenching the Canyon River fault, southeast Olympic Mountains, Washington: Geological Society of America Abstracts with Programs, v. 39, poster No. 22–4.

Wang, K., Mulder, T., Rogers, G.C., and Hyndman, R.D., 1995, Case for very low coupling stress on the Cascadia Subduction Fault: Journal of Geophysical Research. Solid Earth, v. 100, p. 12907–12918, doi:10.1029/95JB00516.

Washington State Department of Ecology, 2015, Washington State Well Log Viewer: https://fortress.wa.gov/ecy/waterresources/map/WCLSWebMap/default.aspx (accessed November 2015).

Wells, R.E., Weaver, C.S., and Blakely, R.J., 1998, Fore-arc migration in Cascadia and its neotectonic significance: Geology, v. 26, p. 759–762, doi:10.1130/0091-7613(1998)026<0759:FAMICA>2.3.CO;2.

Witter, R.C., Givler, R.W., and Carson, R.J., 2008, Two Post-Glacial Earthquakes on the Saddle Mountain West Fault, Southeastern Olympic Peninsula, Washington: Bulletin of the Seismological Society of America, v. 98, p. 2894–2917, doi:10.1785/0120080127.

FIGURE CAPTIONS

Figure 1. Holocene upper plate faults, major drainages, and Cordilleran Ice sheet limit (Thorson, 1989) in the Olympic Mountains, WA. CRF-Canyon River fault; SMFZ - Saddle Mountain fault zone. Inset: Cascadia subduction zone with relative plate motions. JDF - Juan de Fuca plate; PAC - Pacific plate.

Figure 2. Map of the Canyon River fault (CRF) scarps, topographic profile locations, and terrace ages (yellow triangles). A) Vertical separation (Vs) and vertical separation rates (Vsr) across the CRF from terrace profiles. B) Examples of scarp profile vertical separation. C) Profile of Qt5, showing two possible vertical separations across the CRF.

Figure 3. A) Map view of Qt5 terraces. Red and blue gradient shows map view of modeled Canyon River fault (CRF) uplift rate, with local minimum coinciding with the river location. Contours are predicted regional uplift rate (mm/y) from subduction coupling. B) Qt5 tread and strath elevations with uncertainty (shading) versus valley distance. C) Modeled total uplift rate and uncertainty (shading) due to subduction coupling and CRF slip compared to terrace Qt5 incision rates with uncertainty (shading). Inset: Regression of modeled total uplift and incision rate values at >20 km valley distance showing positive correlation.

1GSA Data Repository item 2017xxx, Figures DR1-DR14 and Tables DR1-DR5 and supplementary text (additional model figures, field and sample data, and detailed methods), is available online at http://www.geosociety.org/datarepository/2017/ or on request from editing@geosociety.org.

TABLE 1. OPTICALLY STIMULATED LUMINESCENCE RESULTS

Sample number	Map unit	Location		Elevation (m)	Valley distance (km)	Age ± 2σ (ka)
		Lat (°N)	Long (°W)			
WYN-04	Qt7	47.3423	123.6409	165	5.8	8.9 ± 2.4
WYN-06	Qt5	47.3417	123.6507	194	6.0	14.8 ± 4.0
WYN-07	Qt5b	47.1006	123.6848	57	35.0	14.6 ± 3.5
WYN-08	Qt5	47.0583	123.6928	42	39.8	22.9 ± 6.2
WYN-15	Qt5	47.2121	123.6355	107	20.9	13.5 ± 6.3
WYN-16	Qt5	47.2121	123.6355	109	20.9	13.5 ± 4.0
WYN-17	Qt4	47.3740	123.6147	253	1.2	32.2 ± 9.7
WYN-18	Qt4	47.3740	123.6147	253	1.2	14.7 ± 6.7
WYN-19	Qt8	47.3419	123.6407	162	5.8	7.8 ± 2.4

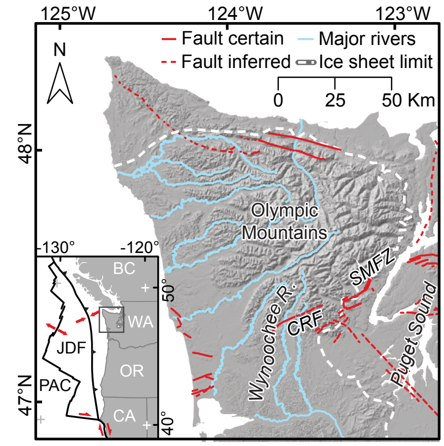

Fig. 1, Delano et al.

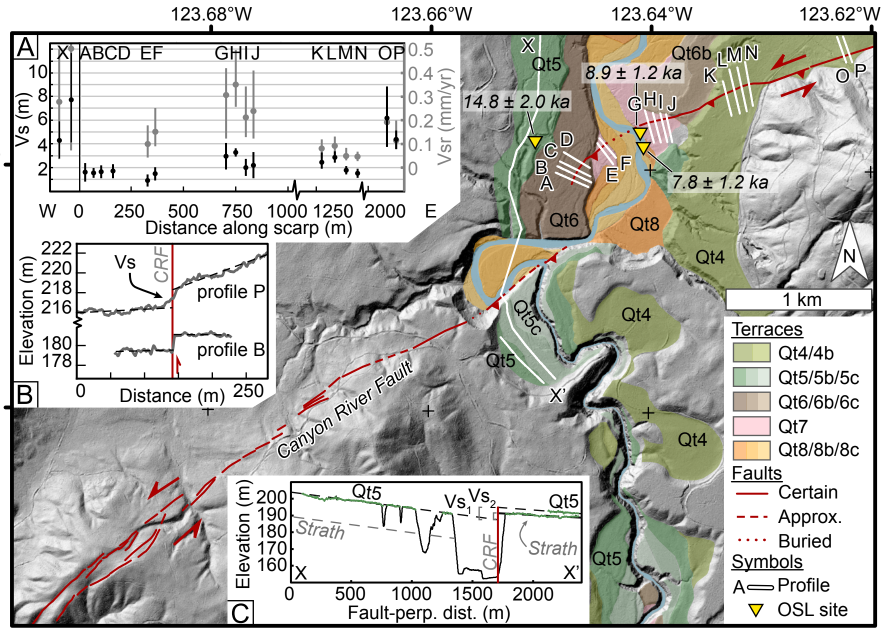

Fig. 2, Delano et al.

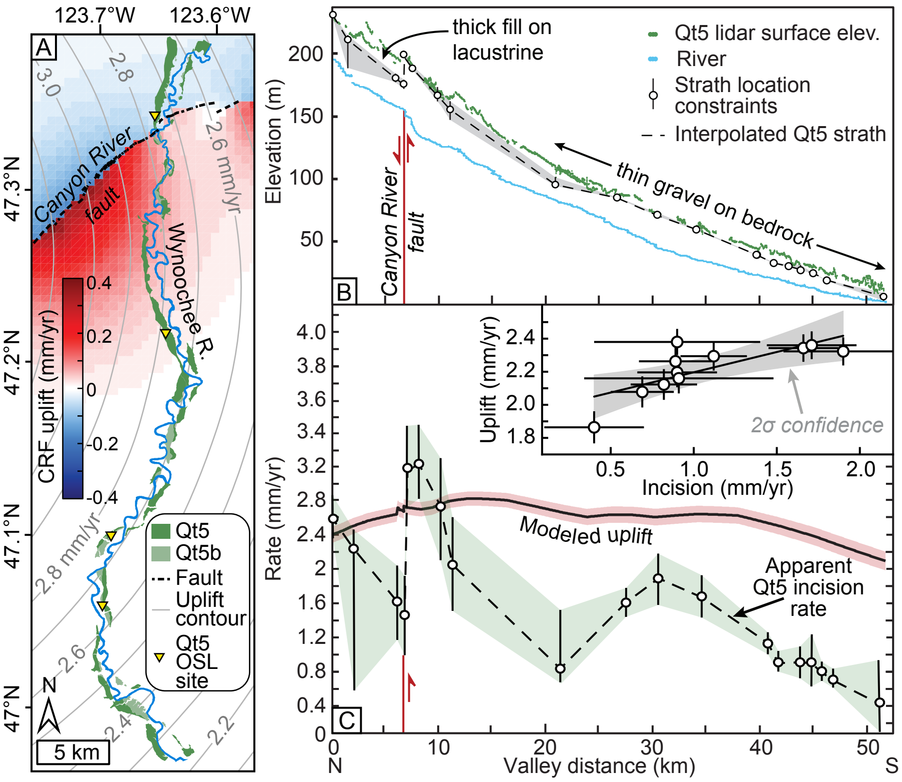

Fig. 3, Delano et al.